JOURNAL OF GEOPHYSICAL RESEARCH, VOL. 97, NO. E5, PAGES 7781–7797, MAY 25, 1992

The Mars Observer Laser Altimeter Investigation

M. T. ZUBER,[1,2] D. E. SMITH,[1] S. C. SOLOMON,[3] D. O. MUHLEMAN,[4] J. W. HEAD,[5] J. B. GARVIN,[1] J. B. ABSHIRE,[1] AND J. L. BUFTON[1]

The primary objective of the Mars Observer laser altimeter (MOLA) investigation is to determine globally the topography of Mars at a level suitable for addressing problems in geology and geophysics. Secondary objectives are to characterize the 1064-nm wavelength surface reflectivity of Mars to contribute to analyses of global surface mineralogy and seasonal albedo changes, to assist in addressing problems in atmospheric circulation, and to provide geodetic control and topographic context for the assessment of possible future Mars landing sites. The principal components of MOLA are a diode-pumped, neodymium-doped yttrium aluminum garnet laser transmitter that emits 1064-nm wavelength laser pulses, a 0.5-m-diameter telescope, a silicon avalanche photodiode detector, and a time interval unit with 10-ns resolution. MOLA will provide measurements of the topography of Mars within approximately 160-m footprints and a center-to-center along-track footprint spacing of 300 m along the Mars Observer subspacecraft ground track. The elevation measurements will be quantized with 1.5 m vertical resolution before correction for orbit- and pointing-induced errors. MOLA profiles will be assembled into a global 0.2° × 0.2° grid that will be referenced to Mars' center of mass with an absolute accuracy of approximately 30 m. Other data products will include a global grid of topographic gradients, corrected individual profiles, and a global 0.2° × 0.2° grid of 1064-nm surface reflectivity.

INTRODUCTION

Surface topography is one of the fundamental measurements required to understand the structure and evolution of solid planetary bodies. Topographic measurements referenced to the planetary center of mass provide a basis for interpreting the gravity field in the context of a planet's internal structure and state of stress. Regional-scale topography and derived topographic gradients are frequently required in investigations of tectonic, volcanic, impact, and surface modification processes. Topography also provides a necessary constraint for atmospheric circulation and climate models. Because of its general importance to so many geoscience disciplines, global characterization of topography was advanced as one of the fundamental goals of NASA's Mars Observer (MO) Mission [*Mars Observer Science Working Group*, 1987].

The topographic objective of the Mars Observer mission will be accomplished using data from the Mars Observer laser altimeter (MOLA). Specific measurement objectives of the MOLA investigation are (1) to derive a global, geodetically referenced 0.2° × 0.2° topographic grid of Mars with a vertical accuracy of better than 30 m suitable for addressing problems in geophysics, geology, and atmospheric circulation; (2) to acquire globally distributed topographic profiles of the Martian surface on short baselines (~100 km) with a vertical precision of better than 2 m suitable for addressing a range of problems in local- and regional-scale geology; and (3) to determine a global 0.2° × 0.2° grid of the 1064-nm wavelength surface reflectivity of Mars to a precision of ~20%, suitable for contributing to studies of global surface mineralogy and seasonal albedo variations.

Present knowledge of the topography of Mars has been derived from several sources and is of widely varying spatial and vertical resolution. Topography has been determined from infrared [*Herr et al.*, 1970] and ultraviolet [*Barth and Hord*, 1971; *Hord*, 1972; *Hord et al.*, 1974] spectroscopy, Earth-based radar observations [*Goldstein and Gillmore*, 1963; *Kotelnikov et al.*, 1963, 1983; *Goldstein*, 1965; *Dyce et al.*, 1967; *Pettengill et al.*, 1969, 1971, 1973; *Downs et al.*, 1971, 1973, 1975, 1978, 1982; *Fjeldbo et al.*, 1977; *Roth et al.*, 1980], radio occultation data [*Cain et al.*, 1972; *Kliore et al.*, 1973; *Christensen*, 1975; *Simpson et al.*, 1977; *Lindal et al.*, 1979] and stereophotogrammetry [*Blasius*, 1973; *Wu et al.*, 1973, 1984; *Wu*, 1978, 1979; *Blasius and Cutts*, 1981]. The Mars Digital Elevation Model [*Wu et al.*, 1986; *U.S. Geological Survey*, 1989], shown in Figure 1, incorporates the above data types and is characterized by a typical horizontal resolution of 1/64° (~1 km at the equator) and vertical errors that range from 500 m near the equator to over 2.5 km near the poles (e.g., Plate 1). The highest-resolution spherical harmonic representation of the topographic field is of degree and order 16 [*Bills and Ferrari*, 1978] and has a coarser resolution than current gravity models [*Balmino et al.*, 1982; *Smith et al.*, 1990*b*]. Much higher resolution topography exists for certain areas from stereophotogrammetric analyses, but these data are not referenced to a global datum and are therefore of limited quantitative utility.

The Mars Observer mission is expected to improve considerably our knowledge of Martian topography. MOLA data should provide a high-integrity, internally consistent long-wavelength topographic field appropriate for addressing geophysical and atmospheric circulation problems. In addition, the topography will be used to derive a global geodetic control grid referenced to Mars' center of mass. MOLA should also produce high-resolution short baseline (~100 km) profiles suitable for addressing many geological prob-

[1]Laboratory for Terrestrial Physics, NASA Goddard Space Flight Center, Greenbelt, Maryland.
[2]Department of Earth and Planetary Sciences, Johns Hopkins University, Baltimore, Maryland.
[3]Department of Earth, Atmospheric, and Planetary Sciences, Massachusetts Institute of Technology, Cambridge.
[4]Division of Geological and Planetary Sciences, California Institute of Technology, Pasadena.
[5]Department of Geological Sciences, Brown University, Providence, Rhode Island.

Paper number 92JE00341.
0148-0227/92/92JE-00341$05.00

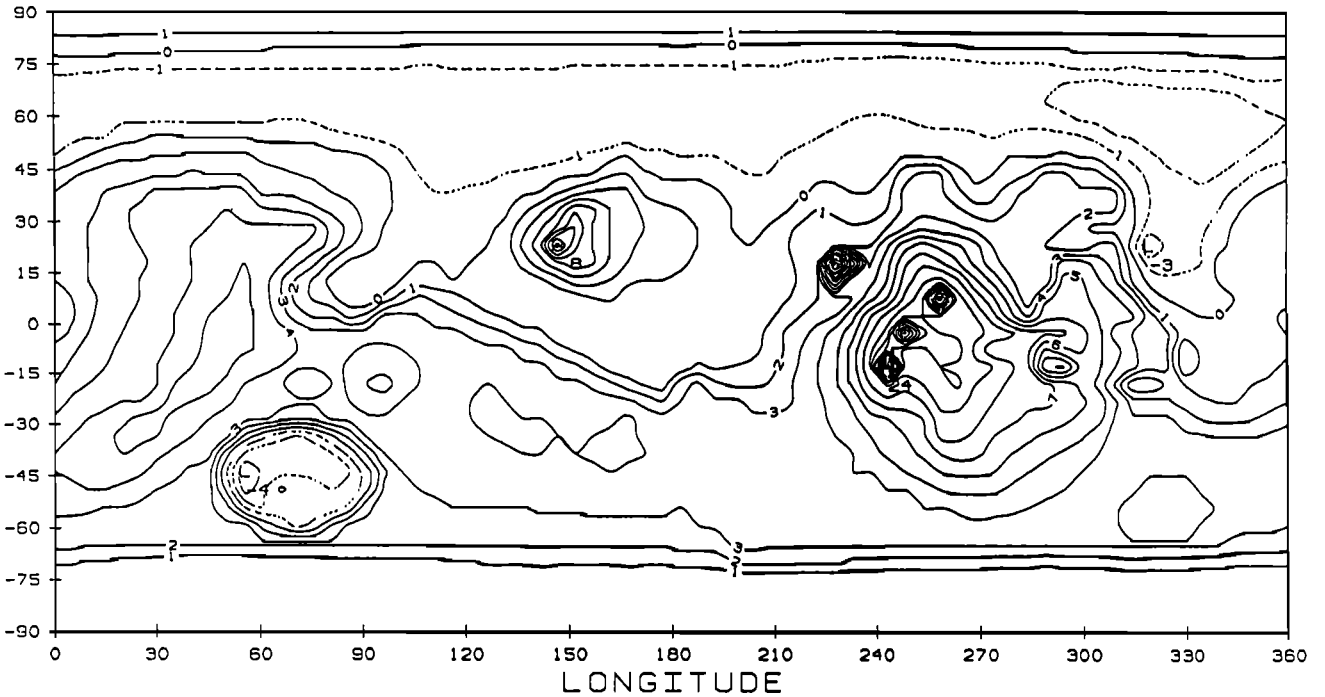

Fig. 1. Mars Digital Elevation Model [after *Wu et al.*, 1986]. Contours are in kilometers. Surface elevations are referenced to the 6.1-mbar atmospheric pressure level. Errors in the elevations range from 500 m near the equator to in excess of 2.5 km at high latitudes.

lems; virtually all types of surface landforms on Mars with length scales greater than 1 km will be sampled, including channels, canyons, lava flows, ridges, graben, craters, cones, landslides, and dunes [*Smith et al.*, 1989]. MOLA data will span a range of spatial scales that will permit analysis, on a global basis, of a broader class of geoscience questions than any previous altimeter investigation, including Earth missions.

SCIENTIFIC OBJECTIVES

The MOLA science team (Table 1) plans a diverse range of scientific studies. For example, Figure 2 lists several discipline areas in Martian geoscience identified by the Committee on Planetary and Lunar Exploration (R. O. Pepin et al., letter to G. Briggs, 1987) that can be addressed with topographic data. These general topics span a broad range of horizontal spatial scales and vertical resolution requirements. Figure 2 also shows the expected vertical resolution of MOLA as a function of horizontal scale. For this resolution spectrum (discussed in more detail in the section on system performance), MOLA data will be adequate to address major questions related to all of the topics in Figure 2. These questions, as well as others that can be investigated using MOLA's measure of 1064-nm surface reflectivity, are discussed in the following paragraphs.

Geodesy

Present knowledge of surface locations on Mars is generally of the order of 1–2 km radially from the planet's center of mass and 1–3 km horizontally [*Davies and Katayama*, 1983; *Davies et al.*, 1992]. The quality of positional knowledge is highest within 30° of the equator and deteriorates rapidly toward the poles. The reference surface for elevation defined as the 6.1-mbar pressure level [*Christensen*, 1975] has an uncertainty with respect to the geometric center of the planet of the order of 1 km [*Davies et al.*, 1992]. A goal of the MOLA and radio science experiments [*Smith et al.*, 1990*a*; *Tyler et al.*, this issue] is to derive simultaneous topography and gravity field models to produce a global geodetic control grid for Mars at a scale of 3 km. The accuracy of the grid is anticipated to be of the order of 30 m radially and 300 m horizontally except for areas within approximately 150 km of the poles, which will not be sampled due to the 92.8° inclination of the MO orbit. If MOLA and the Mars Observer camera (MOC) are aligned to the precision requested by their science teams (though not guaranteed by the MO Project), it should be possible to locate with confidence the positions of MOLA footprints within the field of view of the moderate resolution MOC images. Such positioning information would provide a much needed topographic context for study of geologic features and processes and will aid in the assessment of possible future Mars landing sites.

Isostasy and Internal Structure

Insight into the internal structure and dynamics of a planet and the mechanisms of compensation of topography can be obtained from the relationship between gravity and topography [e.g., *Phillips and Lambeck*, 1980; *Sleep and Phillips*, 1985]. While models derived from potential field data alone are nonunique, they can be evaluated in the context of other observations to study variations of crustal thickness and the distribution of mantle thermal anomalies [*Bills and Ferrari*, 1978; *Banerdt et al.*, 1982; *Sleep and Phillips*, 1985] and the nature of mantle convection [*Schubert et al.*, 1990].

The ratio of gravity to topography as a function of spectral wavelength, when compared with the ratio predicted by flexure of an elastic plate, provides information on the

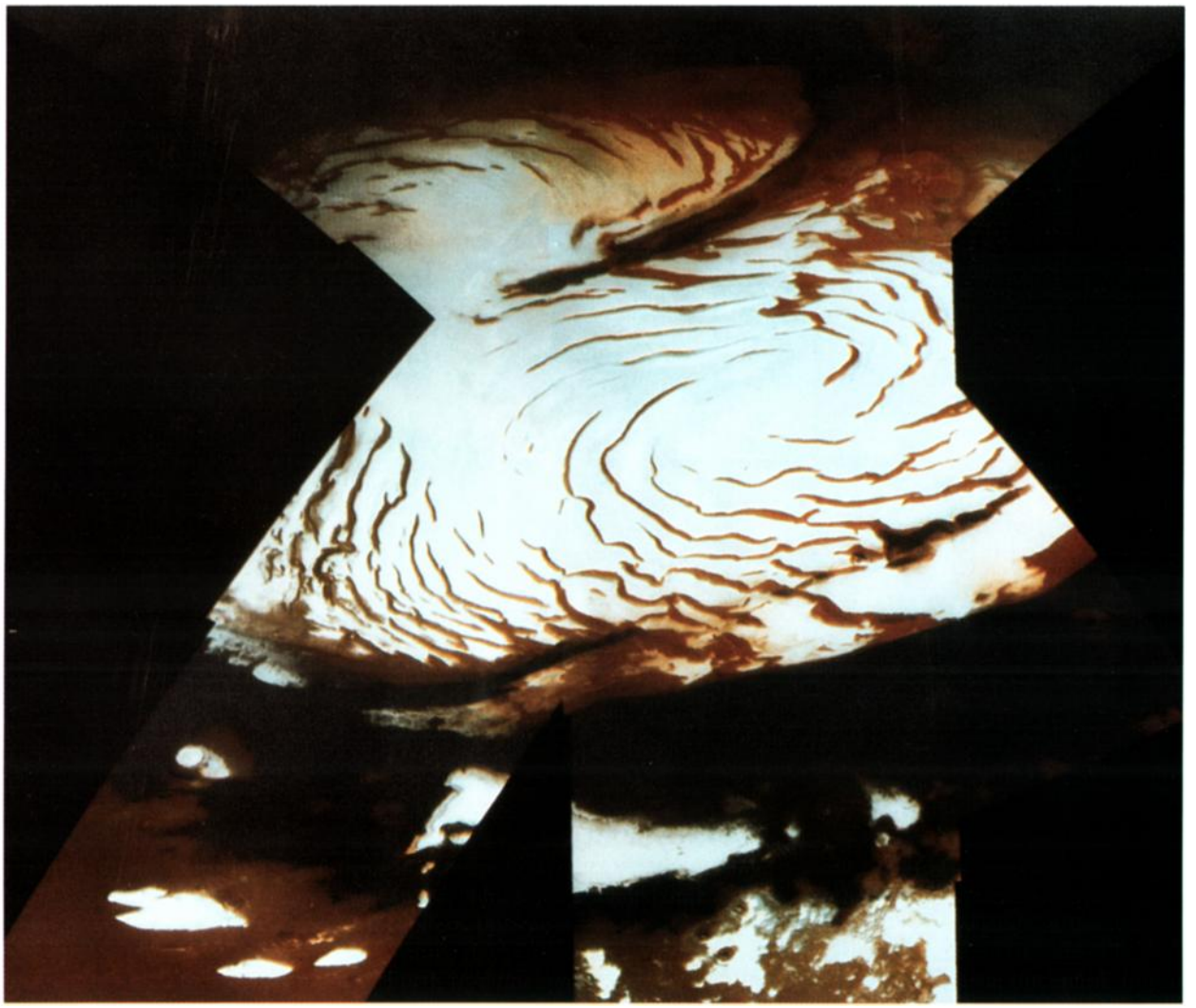

Plate 1. Viking Orbiter mosaic of the north polar cap of Mars. Current topography in this region is characterized by vertical errors of 2.5 km or greater. Image was produced by the U.S. Geological Survey in Flagstaff, Arizona.

thickness of the elastic lithosphere (the rigid outer shell of the planet that can support large stresses over geological time periods) [*Walcott*, 1970; *Forsyth*, 1985]. The lithosphere thickness, or equivalently, flexural rigidity, in the vicinity of large surface loads such as the Martian shield volcanoes can also be inferred by comparing the stresses predicted from flexure models to observed distributions of tectonic features [*Comer et al.*, 1985; *Hall et al.*, 1986; *McGovern and Solomon*, 1990]. With data from MOLA and the MO radio science experiment [*Tyler et al.*, this issue], it may be possible to identify flexural troughs expected owing to loads associated with the major volcanoes, which may provide an additional constraint on lithosphere thickness. Past flexural studies have shown that on average the Martian lithosphere is much thicker than that of Earth [*Phillips and Saunders*, 1975], indicating that Mars has a much lower mean heat flux. With much higher resolution topography it will be possible to map, on a global basis, regional variations in lithospheric thickness and investigate their implications for processes such as convection, mantle plumes, volcanism, and major impacts [e.g., *Solomon and Head*, 1990]. MOLA may also have the capability to identify possible long-wavelength flexure of the lithosphere due to the load of the polar layered deposits [*Zuber*, 1992]. If detected, the structure of the Martian mantle could be better constrained.

Tectonics

MOLA data will play a significant role in the effort to understand better the global-scale tectonics of Mars. For example, consider the hemispheric dichotomy, a distinct (approximately 3 km) elevation difference [*Wu et al.*, 1986; *U.S. Geological Survey*, 1989] between the rugged cratered highlands in the southern hemisphere of Mars and the smooth, more sparsely cratered lowlands in the north. The elevation change across the dichotomy is generally thought to reflect a significant change in crustal thickness. Improved topography and gravity will provide constraints on models that to address whether the dichotomy formed due to an endogenic mechanism such as subcrustal erosion [*Wise et al.*, 1979; *McGill and Dimitriou*, 1990] or an exogenic mechanism such a giant impact or impacts [*Wilhelms and Squyres*, 1984; *Frey and Schultz*, 1988, 1990]. Another enigmatic feature is the Tharsis region, a volcanotectonic

TABLE 1. Mars Observer Laser Altimeter Science and Engineering Teams

Individual	Institution	Role
	Science Team	
D. E. Smith	NASA Goddard Space Flight Center	principal investigator
H. V. Frey	NASA Goddard Space Flight Center	co-investigator
J. B. Garvin	NASA Goddard Space Flight Center	co-investigator
J. W. Head	Brown University	co-investigator
J. G. Marsh	NASA Goddard Space Flight Center	co-investigator
D. O. Muhleman	California Institute of Technology	co-investigator
G. H. Pettengill	Massachusetts Institute of Technology	co-investigator
R. J. Phillips	Washington University, Saint Louis	co-investigator
S. C. Solomon	Massachusetts Institute of Technology	co-investigator
M. T. Zuber	NASA Goddard Space Flight Center	co-investigator
H. J. Zwally	NASA Goddard Space Flight Center	co-investigator
W. B. Banerdt	Jet Propulsion Laboratory	experiment respresentative
	Engineering Team	
B. L. Johnson	NASA Goddard Space Flight Center	instrument manager
J. C. Smith	NASA Goddard Space Flight Center	systems engineer
J. B. Abshire	NASA Goddard Space Flight Center	electronics subsystem manager
J. L. Bufton	NASA Goddard Space Flight Center	sensor subsystem manager
D. W. Hancock	NASA Goddard Space Flight Center/Wallops Flight Facility	ground data system manager
G. S. Hayne	NASA Goddard Space Flight Center/Wallops Flight Facility	performance assessment manager

province that rises up to 10 km above its surroundings and occupies a quarter of the surface area of the planet. With present topography, models for the origin of Tharsis cannot distinguish whether the elevation is primarily a consequence of isostatic uplift [*Banerdt et al.*, 1982] or volcanic construction and lithospheric loading [*Solomon and Head*, 1982; *Willemann and Turcotte*, 1982]. With MOLA's improved topographic resolution it will be possible to assess the relative contributions of these mechanisms to both the topography and to the stress field responsible for Tharsis-related tectonic features such as the Valles Marineris. High-resolution topography will also provide an important basis for understanding the similarities and differences in the origin and evolution of the Tharsis and smaller but similar Elysium province.

Another matter of significant interest is the nature of the stress field that produced various styles of tectonic features [cf. *Banerdt et al.*, 1992]. Topography will provide a constraint on models that can be used to distinguish whether stresses responsible for deformation are global (e.g., due to processes such as planetary thermal expansion/contraction and convection) or regional (e.g., due to flexural loading of individual features) in nature. In addition, topography can be used to investigate the manner in which the stress field has changed through time. For example, topographic profiles across extensional and compressional tectonic features (graben, rifts, and ridges) of a given relative age will permit direct measurements of the magnitudes and distributions of strain associated with specific tectonic episodes.

Volcanism

Images provided by the Mariner and Viking Orbiter spacecraft reveal evidence for pervasive volcanism on the Martian surface [*Carr*, 1973; *Greeley and Spudis*, 1981; *Tanaka et al.*, 1988; *Mouginis-Mark et al.*, 1992]. One of the major goals of the MOLA investigation is to quantify the shapes and thicknesses of volcanic flows and constructs in order to constrain the volumes, styles, and mechanics of Martian volcanism. Gridded and profiled topographic data will permit a global-scale quantitative assessment of the thicknesses, longitudinal and transverse gradients, and detailed relief of major lava fields [e.g., *Lopes and Kilburn*, 1990]. From these parameters, yield strengths and effective viscosities of magmas can be calculated [e.g., *Hulme*, 1976; *Moore et al.*, 1978]. Insight into eruption rates, magma compositions,

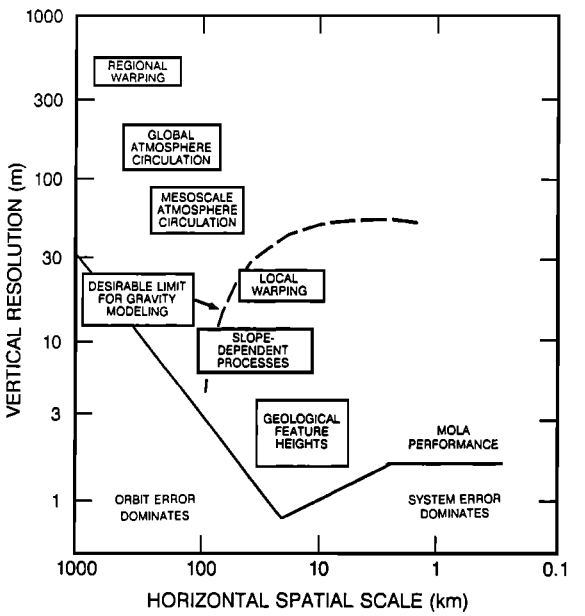

Fig. 2. Vertical resolution requirements as a function of horizontal spatial scale for a range of topics that have relevance to Martian geoscience. The nominal resolution of the Mars Observer laser altimeter (MOLA) data as a function of horizontal spatial scale is shown for comparison. Over the range of spatial scales shown, the resolution of MOLA data should be adequate to address questions related to all of the topics listed. This figure was adapted from a report on Mars Observer altimetry options by the Committee on Planetary and Lunar Exploration (R. O. Pepin et al., letter to G. Briggs, 1987).

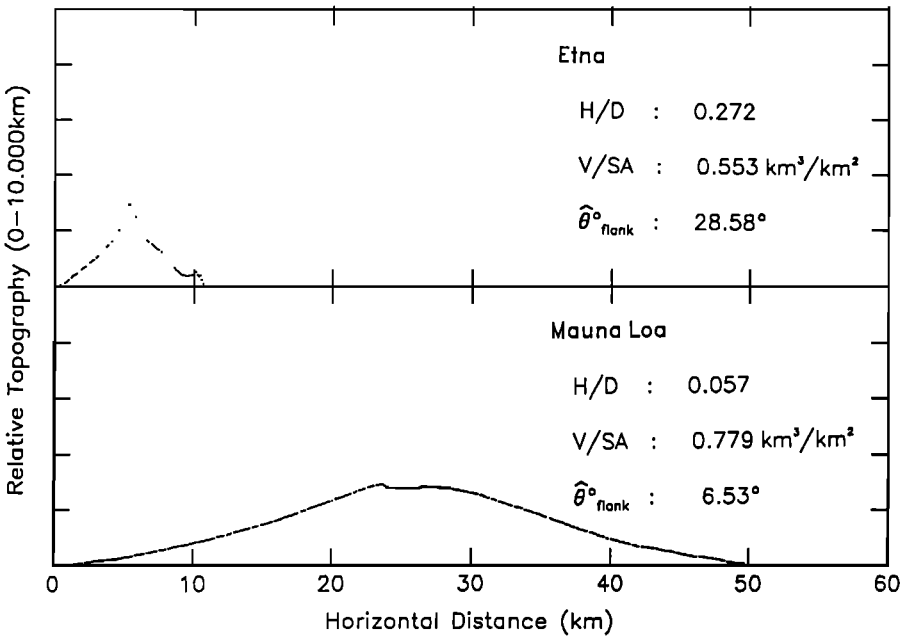

Fig. 3. Digital topographic profiles of two terrestrial volcanoes, Mount Etna, Sicily, (top) and Mauna Loa, Hawaii, (bottom) resampled at approximately Mars Observer laser altimeter (MOLA) spatial resolution. The profiles were constructed assuming 100-m footprints spaced at least 330 m apart. The number of points plotted is governed by the MOLA ranging probabilities in Table 3 and depends on the 100-m baseline surface slopes. For slopes < 12°, 90% of the points are plotted; for slopes between 12° and 27°, 50% of the points are plotted; and for slopes > 27°, 10% of the points are plotted. For each volcano the height/basal diameter (H/D) and volume/surface area (V/SA, determined assuming axisymmetry) ratios are given along with the average flank slope $\hat{\theta}$. These parameters, as well as others that can be measured with MOLA, contain information on the characteristics, style, and duration of the eruption process. For the observed distributions of the 100-m slopes and assuming nominal atmospheric conditions and system operation, MOLA is likely to detect approximately 58% of the transmitted laser pulses for a volcano similar in shape to Mount Etna and approximately 89% for a volcano similar to Mauna Loa. Steep-sloped surfaces such as the flanks of Mount Etna are not anticipated to be common on Mars, though MOLA should provide useful measurements of topography even on such rough surfaces. The maximum errors in H/D and V/SA calculated from the profile of Mount Etna with MOLA's ranging probabilities compared with values calculated from a profile in which no laser pulses are lost are each only 3%.

volatile contents, flow dynamics, and the depths of magmatic source regions [*Wilson and Head*, 1981; *Greeley and Crown*, 1990] should be possible. These will contribute to a better understanding of the spatial and thermal structure of the Martian interior. Paleoslopes inferred from the flow directions of ancient lava flows (or stream channels), when compared with present-day slopes, can provide a measure of postemplacement changes in relief associated with tectonism [*Mouginis-Mark et al.*, 1982]. Subtle volcanic constructs, such as low-relief lava shields which may be pervasive on the northern plains, may be uniquely detectable from MOLA profiles. Knowledge of the detailed topography of volcanic constructs can be used to understand better edifice processes such as caldera subsidence and magma chamber inflation and deflation (M. T. Zuber and P. J. Mouginis-Mark, Caldera subsidence and magma chamber depth of the Olympus Mons volcano, submitted to *Journal of Geophysical Research*, 1992). Quantitative analysis of the shapes of volcanic craters may also be used to identify volcanic areas in which volatiles were present at the time of eruption. In addition, measurements of parameters such as the aspect ratio (height/basal diameter, H/D), average flank slope ($\hat{\theta}$), and ratio of volume to surface area (V/SA) of volcanic constructs can be related to the complexity and style of volcano growth through time [cf. *Garvin and Williams*, 1990]. These parameters are calculated in Figure 3 from profiles of two terrestrial volcanoes at MOLA's approximate resolution. The values illustrate the gross morphological differences between Mount Etna, an andesitic stratovolcano, and Mauna Loa, a composite tholeiitic shield.

Geology and Geomorphology

Virtually all geologic processes involving flow of materials require knowledge of topography and topographic gradients. The dynamics of erosional processes on Mars involving wind, water, and ice strongly influence the development of global Martian climatic cycles. Key questions related to the physics of surface processes typically are concerned with regional slopes on baselines of tens of kilometers or less [*Baker*, 1982]. For example, to resolve basic questions such as the extent of slope control in mass wasting, a high-integrity global topographic model is necessary. Together with precise slopes, a knowledge of parameters including heights, widths, depths, and rim heights of such fundamental landform types as graben, ridges, channels, and craters permit quantification of landform degradation as a means of understanding past climates. Elevation and slope data can be used in conjunction with morphology determined from imaging to constrain processes of formation, emplacement, and degradation of diagnostic landforms (compare Figure 2). For example, the intensity and net effect on the surface of regional eolian processes are strongly controlled by both slopes and major topographic obstacles [*Scheiddeger*, 1970].

If sufficiently large obstructions to near-surface flow exist, certain deposition patterns will develop. Wind tails, moats, and other phenomena depend on the nature of obstructions in the windstream and may develop in a given location as a function of Martian climatic cycles.

Volatiles and Polar Processes

In areas that have not undergone subsequent tectonic deformation, knowledge of topographic gradients will permit the determination of surface fluid flow directions and will enable the identification of possible source regions of ancient channels. Topographic characterization of the geometries of channels will permit better understanding of flow properties and dynamics, providing important information on Martian paleoclimates, aeolian, fluvial and pluvial cycles, and sources and sinks of Martian volatiles [*Baker and Milton*, 1974; *Sharp and Malin*, 1975; *Carr*, 1979; *Baker*, 1982]. Determination of slopes in ancient terrains will be used to identify areas where liquid water may have ponded early in Martian history.

Currently, the topography in the Martian polar regions, such as shown in Plate 1, is known to no better than 2.5 km. However, given the polar orbit of Mars Observer, the high-latitude regions will be mapped at the highest spatial resolution on the planet. Orbital track spacings at latitudes within 5° of the poles (with the exception of areas not sampled due to the inclination of the MO orbit) will be of the same order as the width of MOLA footprints. From the dense topographic grids at high latitudes in combination with improved gravity to be provided by MO [*Tyler et al.*, this issue], it will be possible to estimate accurately the thicknesses and volumes of the polar caps [e.g., *Zwally et al.*, 1989] and thus constrain the present volatile inventory. It may also be possible to resolve the thicknesses of the layered terrains, shown in Plate 1. This would provide information on the polar cap volume as a function of time, which would constrain models of Mars' climatic history. In addition, the present topography of the polar caps can be compared with that of mantling deposits at mid-latitudes that are proposed to be the site of ancient polar deposits [*Schultz and Lutz*, 1988]. Depending on the seasonal deposition and sublimation volumes and the knowledge of the MO orbit, it is possible that seasonal height changes in the polar caps, as predicted by mass balance models [e.g., *Haberle and Jakosky*, 1990], could be measured.

Since rock, dust, and ice are characterized by different 1064-nm reflectivities, measurements of MOLA's received/transmitted pulse energies over time will allow the seasonal extent of the caps to be determined. In addition, the single-scattering albedo will be strongly affected by dust and will vary from near unity to perhaps as low as 0.5. These data, combined with visible albedo and surface thermal emission measurements [*Christensen et al.*, this issue], may offer unique information about both the dust and the ices.

Impact Processes

The detailed shapes of simple and complex impact craters provide important information on the mechanics of impact, the structure of impacted substrate, the volumes of material excavated, the emplacement of ejecta, and the nature of subsequent surface modificational processes. For example, morphological parameters (e.g., depth, diameter, ejecta thickness, rim height, and interior volume), especially for pristine simple crater forms, will provide important constraints on the mechanics of the cratering process as a function of target properties and gravity [*Pike*, 1977]. For degraded craters these parameters contain information concerning erosional and climate histories [*Chapman and Jones*, 1977]. Subtle morphologic differences between smaller craters, detectable by means of MOLA profiles, should allow discrimination between those of impact and volcanic origin, hence permitting relative age estimates in complex terrains to be improved.

The topographic shapes of impact craters and basins are sensitive indicators of the depth distribution of the mechanical strength of the lithosphere [cf. *Solomon et al.*, 1982]. In areas where craters have not been significantly infilled by aeolian deposits, craters shapes can be used, in combination with models of viscous relaxation of topography, to constrain fundamental properties of the Martian interior such as the thermal gradient and crustal thickness [*Grimm and Solomon*, 1988]. Basin-scale impacts significantly perturbed the early thermal state of the lithosphere and must have played a significant role in the early thermal evolution of Mars. The subsurface structure associated with an impact basin, as determined by topography and gravity [*Phillips and Dvorak*, 1981; *Sjogren and Wimberly*, 1981; *Solomon et al.*, 1983], can be used to help constrain the extent of possible present-day thermal perturbation of the mantle, as well as the depth of excavation and the amount of elastic rebound associated with the impact event. Better understanding of the mechanics of large impacts, which also requires detailed modeling and subsurface seismic, structural, and geologic information, can provide a basis for evaluating their importance relative to that of internal dynamics in contributing to the early heat budget of Mars.

Atmospheric Particulates, Clouds, and Hazes

The 1064-nm laser energy from MOLA will interact most strongly with 100- to 1000-nm-diameter particles in the Martian atmosphere. The interaction will be dominated by scattering but will be characterized by a strong component of absorption for silicate and magnetite particles. Carbon dioxide and water ice will exhibit nearly conservative scattering, in which photons scatter many times without significant energy loss. The total atmospheric opacity sensed by MOLA will be similar to, but somewhat less than, the visual opacity, which is near unity under normal conditions but 5 or more during dust storms [*Pollack et al.*, 1979]. For dense water ice clouds, hazes, or fogs in which particles are mostly backscattering and opacity rapidly increases with depth, detection may be possible. Measurements of the heights of dense water ice clouds or fogs would provide unique information on the vertical structure of the Martian atmosphere.

Atmospheric Circulation

Surface topography is a required boundary condition in models of atmospheric circulation. On the global scale, elevation data from MOLA will be used to quantify topographic asymmetries between the poles that influence global circulation patterns and quasi-periodic climate changes [*Pollack et al.*, 1981]. Regional-scale topography will be used to

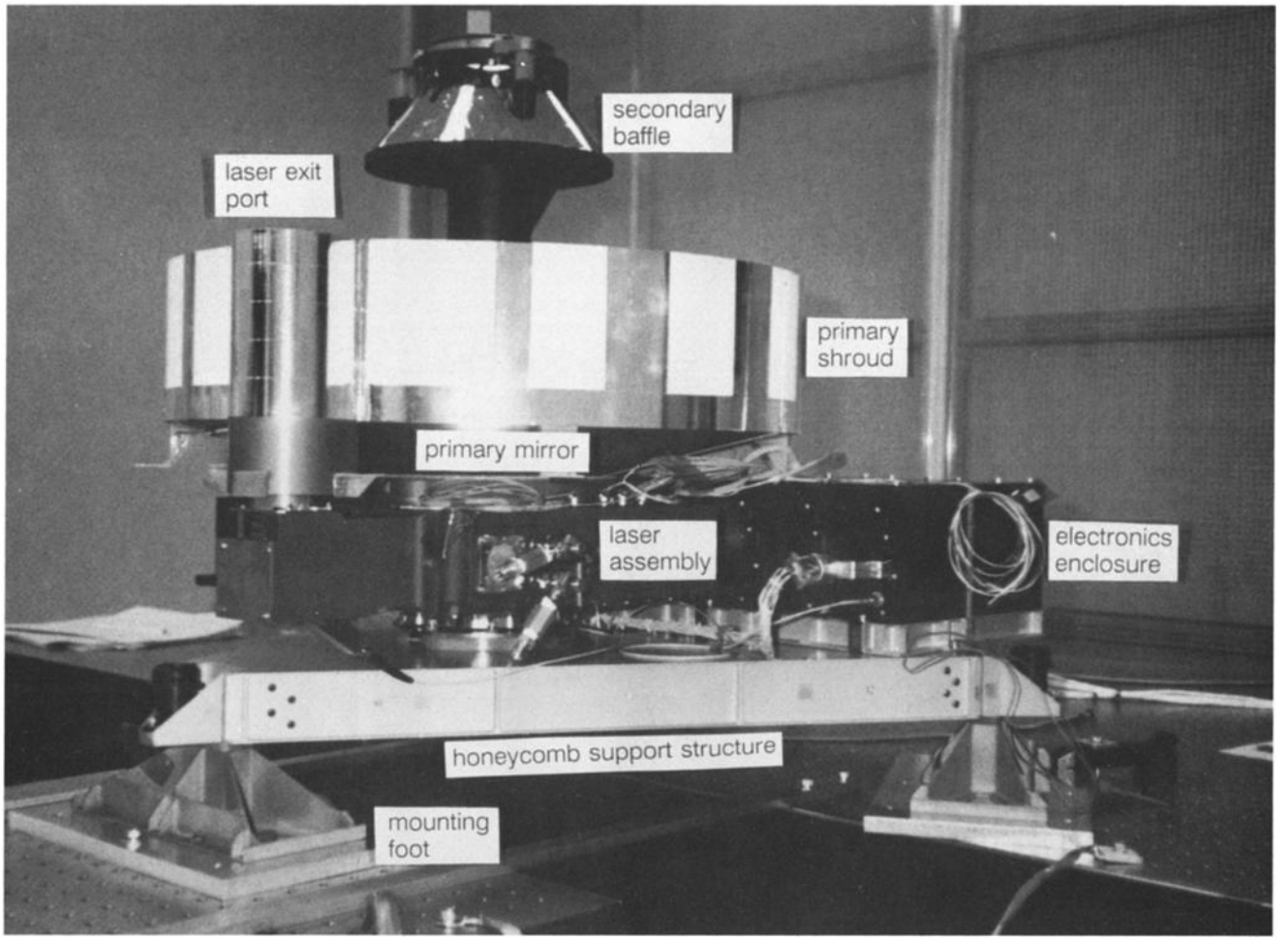

Fig. 4. Mars Observer laser altimeter. The primary mirror has a diameter of 0.5 m.

understand better the nature of mesoscale circulation. For example, regions of elevated topography affect atmospheric winds by acting both as obstacles to flow and as heat sources and sinks [*Pollack*, 1989]. Breaking of gravity waves related to regional-scale topography induces turbulent mixing of atmospheric constituents and may influence latitudinal thermal gradients in the mesosphere [*Holton*, 1983; *Barnes*, 1990]. Knowledge obtained on the patterns of Martian winds and near-surface wind stresses will have relevance in assessing future landing site selection and safety.

INSTRUMENT DESCRIPTION

Ranging Approach

The MOLA instrument, shown in Figure 4, will measure the round-trip time of flight of infrared laser pulses transmitted from the Mars Observer spacecraft to the Martian surface. The instrument normally operates in a single autonomous mode, in which it will produce ranging measurements. Surface topography estimates can be derived from these, given appropriate corrections for the position and attitude of the spacecraft.

Figure 5 shows a schematic illustration of MOLA's ranging procedure. The instrument measures range by transmitting a single pulse of 1064-nm wavelength laser radiation with a known peak power (represented as P_o) and duration (represented as W_o) at time T_o in a direction ideally normal to the Martian surface. The pulse is reflected from the surface, and some fraction of the laser energy is backscattered in the direction of the spacecraft. The received pulse is detected (see below) above the 1064-nm solar background and system electronic noise threshold at time T_R. A range gate is used to enhance sensitivity by allowing detection only during the period of time which the return pulse is expected. Optical scattering due to the finite depth of the surface within the transmitted beam causes the received pulse to be increased in width (W_R) and decreased in power (P_R) compared to the transmitted pulse. The range to the surface, Z, is determined from the two-way travel time ($\Delta T = T_R - T_o$) by

$$Z = \frac{c\Delta T}{2n} \tag{1}$$

where c is the vacuum speed of light and n is the group index of refraction of the Mars atmosphere at 1064 nm. The round-trip propagation time of the laser pulse is measured with a time interval unit (TIU), which is activated when the pulse is transmitted and stopped when a specified threshold of the backscattered laser pulse is received within the range gate. The 1064-nm surface reflectivity is estimated from the ratio of the received pulse energy to the laser exit pulse energy, given a correction for the assumed opacity of the

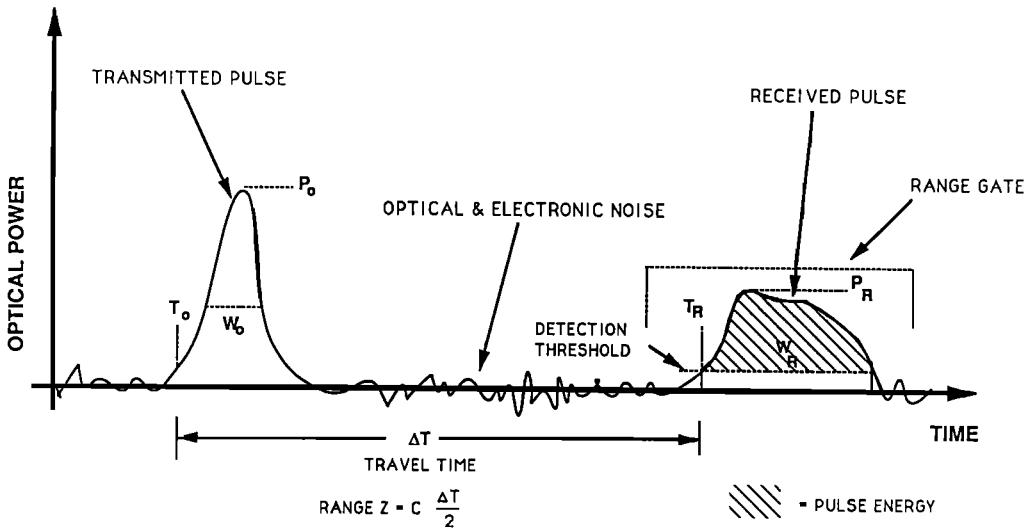

Fig. 5. Schematic illustration of the ranging approach of the Mars Observer laser altimeter (MOLA). The instrument transmits a laser pulse with power P_o and duration W_o at time T_o. The pulse is reflected from the surface and detected by MOLA above the background and electronic noise threshold at time T_R. The received pulse has a lower power P_R and a longer duration W_R than the transmitted pulse due to its interaction with the Martian surface. The range to the surface Z is determined from the time of flight of the pulse ΔT divided by 2 times the group index of refraction of the atmosphere n, multiplied by the speed of light c. The pulse energy corresponds to the area under the pulse above the detection threshold, shown for the received pulse by the diagonally striped area. The received pulse is detected in a range gate that represents a period of time during which the pulse is expected.

Martian atmosphere at 1064 nm. The received pulse energy is determined by integrating the area under the received pulse above the detection threshold. The detection threshold and the width and position of MOLA's range gate were designed to be adjustable to maximize the probability of detection.

Each transmitted laser pulse may result in a unique, high-resolution measurement of range. This is in contrast to most radar altimeters, which require extensive pulse averaging to achieve high vertical precision [cf. *McArthur*, 1978]. The difference in the operation of these systems is a consequence of the relative wavelengths of the transmitted electromagnetic radiation, the diameter of the transmitter antenna, the transmitted peak power of each instrument, and the diameter of the transmitted beam on the reflecting surface. For a radar altimeter all of the length scales are similar, resulting in coherent fading or speckle modulation which can cause significant noise on a single received pulse. This effect is reduced by statistically averaging many pulses to make a single measurement. In contrast, for MOLA, the wavelength of the transmitted signal is many orders of magnitude less than the diameter of the transmitted beam and the diameter of the receiving telescope, so speckle is not important. Due to this and the high transmitted peak power (~1 mW), the signal-to-noise ratio is sufficiently high for a single laser pulse so that one pulse can provide a unique measurement of range.

All components of MOLA except for the laser and telescope are being designed, built, and tested at NASA's Goddard Space Flight Center (GSFC). The lead engineers are listed in Table 1. The telescope is a flight-quality spare from the Voyager infrared interferometer spectrometer (IRIS) instrument originally built by Texas Instruments, Dallas, Texas. The laser was designed and built at the Laser and Electronics Systems Division of McDonnell-Douglas Electronic Systems Company, Saint Louis, Missouri. The primary components of the instrument and the instrument operation are briefly described below and illustrated in the functional diagram in Figure 6. The instrument parameters are summarized in Table 2.

Ranging Operation

MOLA's transmitter is a Q-switched, neodymium-doped yttrium aluminum garnet (Nd:YAG) laser oscillator which is pumped by a 44-bar laser array. Each bar contains ~1000 AlGaAs (aluminum, gallium arsenide) laser diodes. The Q-switch controls the pulsing of the laser, and Nd:YAG refers to the composition of the material that is optically excited to produce laser action. The laser emits 7.5-ns-wide (full width at half the maximum pulse amplitude, FWHM) pulses at 1064 nm. The pulse repetition rate is 10 Hz, and the expected pulse energy is 40 mJ at the beginning of mapping and 30 mJ at end of mission. The laser consumes 13.7 W when operating, and its on-orbit lifetime is expected to be at least 6×10^8 laser pulses (~2 years).

Figure 6 outlines the instrument operation. The ranging process initiates with the laser firing at a rate controlled by a 100-MHz oscillator. The reference laser pulse energy is determined by optically sampling the center portion of the laser exit beam via transmission optics and passing the signal through an energy monitor. The collected energy is focused onto a single-mode 0.1-nm fiber optic cable and is relayed onto the silicon photodiode start-detector located within the MOLA electronics box. The start-detector threshold level is set via software as a control constant and is not normally adjusted during MOLA science mode operation. The output of the start detector acts to initiate the range timing process by starting the TIU.

The altimeter receiver utilizes a 0.5-m-diameter, nickel-

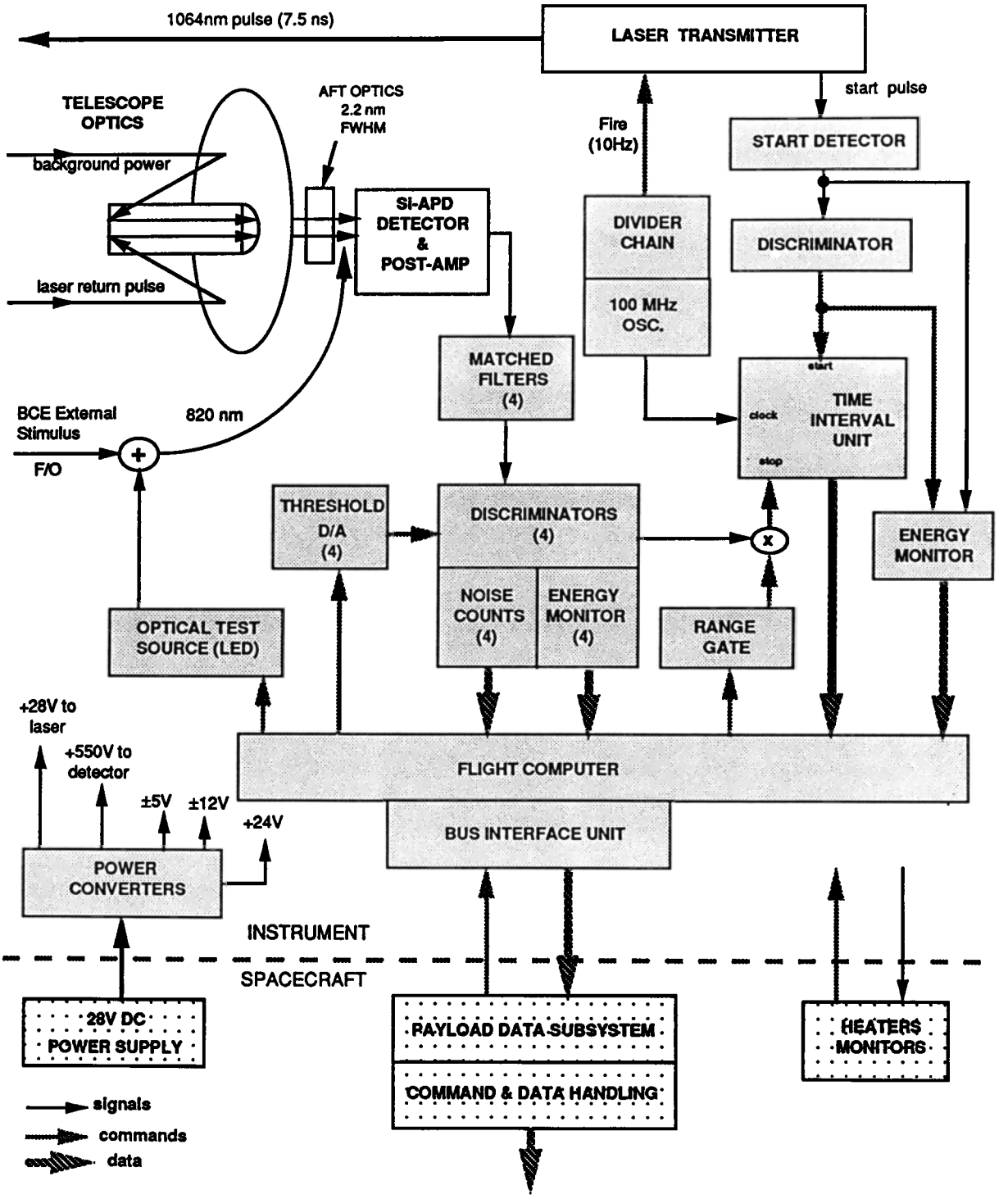

Fig. 6. Mars Observer laser altimeter functional diagram.

plated, gold-coated beryllium telescope. The received laser pulse, after being focused by the telescope's primary and secondary mirrors, is recollimated by a small meniscus lens and passes through a 2.2-nm-wide optical bandpass filter which is used to reject solar background. The laser signal is then focused by a second meniscus lens onto a silicon avalanche photodiode (Si APD) detector which has a 40% quantum efficiency at 1064 nm. After passing through a low-noise preamplifier, the received signal passes through a parallel bank of four low-pass filters. These filters have Gaussian shapes and are matched for received pulse widths of 20, 60, 180, and 540 ns (Table 3). The widths of these matched filters were selected to optimize detection probabilities for Mars footprint-scale surface slopes of 1.7°, 5°, 15°, and 39°, though all slopes from 0° to greater than 39° will be detectable with various probabilities. The thresholds of the four receiver channels are continuously computed and updated once every second to maximize detection probabilities

TABLE 2. Mars Observer Laser Altimeter Instrument Parameters

Parameter	Value
Physical Characteristics	
Volume, m^3	0.15
Mass, kg	26.18
Power, W	28.74
Laser Transmitter	
Laser type	Q-switched, diode-pumped Nd:YAG
Wavelength, nm	1064
Laser energy, mJ $pulse^{-1}$	40–30*
Laser power consumption, W	13.7
Pulse width (FWHM), ns	7.5
Pulse repetition rate, s^{-1}	10
Beam cross section, mm^2	25 × 25
Beam divergence, mrad	0.3
Altimeter Receiver	
Telescope type	Cassegrain
Mirror composition	gold-coated beryllium
Telescope diameter, m	0.5
Focal length, m	0.74
Detector type	silicon avalanche photodiode (Si APD)
Sensitivity, nW	1
Optical filter, nm bandpass	2.2
Field of view, mrad	~0.85
Receiver Electronics	
Receiver type	match-filtered leading edge tracker
Time resolution, ns	10
Range resolution, m	1.5
Pulse energy resolution	±2%
Measurements	
Footprint size, m	160
Footprint spacing (center to center, along track), m	300
Computer	
Type	80C86
Data rate, bits s^{-1}	617.14

Nd:YAG is neodymium-doped yttrium aluminum garnet. FWHM is full width half maximum.
*Values at start and end of mapping sequence.

and minimize false returns. If any of the filter outputs exceed the specified detection threshold within the range gate, the signal triggers a voltage comparator circuit, which stops the TIU. The TIU measures the transit time of the laser pulse with 10-ns (1.5-m) resolution. The received energies of the channel that stops the TIU and the next adjacent channel, along with the background noise counts, are measured by a second energy monitor and subsequently reported to the MOLA packet data via the flight computer. The transmitted and received energies are measured with 2% resolution.

The matched filters utilized in the altimeter receiver constitute a new approach for estimating within-footprint terrain height variations and footprint-scale surface slopes. Airborne laser altimeters sometimes utilize waveform digitizers, which measure the returned signal power as a function of time and thus provide a discrete representation of the received waveform. The shape of the waveform yields information on the footprint-scale roughness of the surface, with smooth, flat surfaces exhibiting narrow waveforms (W_R in Figure 5) with high peak powers (P_R in Figure 5), and rough, sloping surfaces characterized by broad waveforms with low peak powers.

MOLA's strict power and data rate constraints, in combination with the desire to minimize the amount of onboard data processing, precluded the inclusion of a waveform digitizer. Instead, the received pulse is passed in parallel through four filters matched to returned pulse widths that correspond to a broad range of terrain height variations (Table 3). MOLA's matched filters serve two purposes. First, convolution of the signal with a given filter reduces noise and maximizes the likelihood of a pulse detection. Second, the output of the filter channel which first exceeds threshold triggers the TIU. This provides a one-in-four-bin estimate of the height variation of the terrain within the footprint. The pulse energies of both the channel that triggers the TIU and the following triggering channel are retained in the data stream. Their information will be used in ground-based processing to correct for pulse-spreading-induced ranging errors and improving the estimate of terrain height variations.

Technological Challenges

The development of a space-qualified, long-lifetime laser represents one of the primary engineering challenges associated with MOLA. For comparison, the ruby flashlamp laser altimeters flown on the Apollo 15, 16, and 17 missions [*Kaula et al.*, 1972, 1973, 1974] each operated for less than 10^4 laser pulses. High-pulse-repetition-rate lasers with lifetimes of the order of 10^9 shots have been made possible due to breakthroughs in solid-state laser technology, resulting in improvements in the peak power, brightness, and availability of semiconductor diodes and arrays [*Cross et al.*, 1987; *Byer*, 1988]. The key technological advance has been the replacement of the flash lamp, which is the device that has traditionally been used to pump optical energy into the laser rod, with a highly efficient array of laser diodes. While flash lamp lasers fail catastrophically, diode-pumped lasers such as MOLA's instead undergo a gradual degradation in energy output as individual diodes fail. Laser diodes also produce the required pump energy only in a region near the laser rod's absorption band, which dramatically improves the laser's electrical to optical efficiency.

SYSTEM PERFORMANCE

Resolution

The along-track horizontal resolution of MOLA is dictated by the divergence and pulse repetition frequency of the laser (Table 2), and the altitude, velocity, and pointing control of the spacecraft. The first and third quantities dictate that the size of the laser footprint on the surface will be approxi-

TABLE 3. Mars Observer Laser Altimeter Matched Filter Characteristics

Characteristic	Channel 1	Channel 2	Channel 3	Channel 4
Description	smooth	moderate	rough	scarp
Channel width, ns	20	60	180	540
Terrain height variation within footprint, m	3	9	27	81
Footprint-scale surface tilt, deg	1.1	3.3	9.8	27.0
Probability of measurement	0.9	0.9	0.5	0.1

mately 160 m. All of these factors combine to indicate that the spacing between the centers of successive footprints will be approximately 300 m, so for MOLA's profiles less than one half of the 160-m-wide swath along the ground track will be sampled. The across-track resolution is determined by the footprint size and the details of the spacecraft orbit and pointing. For the MO orbit [cf. *Albee et al.*, this issue] and a nominal 687-day mission (one Martian year) the maximum track spacing is at the equator and at the end of mission would equal, on average, about 1.6 km. To account for possible data loss and to assure adequate sampling statistics within each grid cell, global grids of topography and surface reflectivity are planned to be a factor of 7 coarser than the average track spacing at the end of the nominal mission.

The vertical precision of MOLA is dictated by the laser pulse width, the timing resolution of the TIU, the spacecraft pointing control and knowledge, and the footprint-scale roughness of the Martian surface. In laser altimetry, narrow laser pulses are favored to minimize the reduction in amplitude of the pulse as it is spread in time due to interaction with the nonideally reflecting surface (and possibly with the atmosphere as well). The 7.5-ns FWHM laser pulse width of MOLA, coupled with the 10-ns resolution of the time interval unit, determines the range quantization level of MOLA to be 1.5 m under best case conditions, that is, when ranging to a flat surface (slope $< 2°$) while the MO spacecraft points directly at nadir. For mean surface slopes $> 2°$ (or equivalent height variations within the footprint) the vertical precision can be comparable to approximately 10% of the elevation change within the footprint given an accurate estimate of the received optical pulse width. Errors due to nonnadir pointing of the MO spacecraft are of the order of 0.20 m mrad^{-1} on a flat surface [cf. *Bufton*, 1989] but increase to many tens of meters for the level of pointing control guaranteed for the MO spacecraft. However, the actual pointing knowledge is expected to be considerably better than the guaranteed values [*Mars Observer Science Working Group*, 1989]. Pointing errors will be correctable to varying extents from MO precision orbit determination [*Smith et al.*, 1990*a*]. Nonetheless, footprint-scale surface roughness and gradients and spacecraft pointing effects are anticipated to constitute significant sources of error in the absolute determination of range. However, as shown in Figure 2, for spatial scales of the order of 1–10 km, errors can be reduced by statistically averaging range measurements. The expected improvement in vertical resolution is of the order of $n^{-1/2}$, where n is the number of measurements. The limiting extent to which accuracy can be improved depends on the detailed nature of the sources of random error. Figure 2 assumes that statistical averaging can result in no more than an order of magnitude improvement in accuracy over the value for a single measurement.

The limiting vertical accuracy to which MOLA will measure Martian topography will be determined predominantly by the accuracy to which the radial orbital position of the Mars Observer spacecraft is known. The dominant error sources in the determination of the MO orbit are uncertainties in the gravitational field, atmospheric density, solar radiation pressure, and perturbations caused by desaturations of the MO spacecraft momentum wheels. (Adjustments of spacecraft attitude are accomplished using momentum wheels which become saturated over time. Desaturation of the momentum wheels is accomplished using small thrusters that induce small nongravitational accelerations in the spacecraft orbit.) Current knowledge of the Mars gravity field is limited to tracking data collected from the eccentric orbits of Mariner 9, Viking 1, and Viking 2 [*Esposito et al.*, 1992]. Even after advanced reprocessing of these data [*Smith et al.*, 1990*b*], the gravity model is accurate in the radial direction only to about 70 m (rms) for the nominal MO orbit. Tracking data from the polar, ~400-km elevation, near-circular orbit of MO will greatly improve our current knowledge of the Martian gravity field. Simulations suggest that the radial errors in the MO orbit due to errors in the gravity field will be reduced to about 10 m (rms) after improving the gravity field model with tracking data from MO [*Smith et al.*, 1990*a*]. This error is commensurate with the combined errors due to other uncertainties. As illustrated in Figure 2, most of the error in the orbit computations occurs at long wavelengths, so that short-wavelength variations in the topography measured by MOLA will be dominated by system error and will be largely unaffected by orbit error.

Link Analysis

Successful ranging to the Martian surface using MOLA will require an adequate signal-to-noise ratio. In laser altimetry the performance of the system can be estimated by calculating link margins, which quantify the amount of laser energy in excess of that required in order to measure range with a given probability under a given set of conditions. Link margins are given in decibels and are usually referenced to the transmitted signal. Positive link margins indicate that the system will provide stronger signals than required, and that the system performance should exceed the requirement. Independent link analyses have been undertaken by the MOLA electronics team at GSFC and at Johns Hopkins University (F. Davidson, unpublished data, 1991) to estimate MOLA's performance under expected and worse-than-expected Mars conditions.

Figure 7 illustrates the conceptual approach for determining the system performance and shows assumed probability density distributions of the matched filter outputs, with the detector noise only on the left and the corresponding signal plus background outputs on the right. Cases are shown for daytime and nighttime conditions. The performance calculation assumes a Gaussian model for the filtered detector output. The performance can be described by four numbers per filter channel, representing the widths (σ_0 and σ_1) and mean values (μ_0 and μ_1) of the probability distributions. The mean values of both distributions shift toward the left for low solar background and to the right for high solar background.

For a given set of conditions the probability of making a successful range measurement (P_{meas}) can be expressed as functions of the probability of detection (P_{det}) and the probability of a false alarm (P_{FA}) as

$$P_{meas} = P_{det}(1 - P_{FA}) \tag{2}$$

where a false alarm represents a trigger due to background noise. In practice, MOLA is designed to maximize the probabilities of detected measurements and minimize false alarms.

In determining the system performance the most important parameter is the mean detected signal level (N_r, in photoelectrons) which is given by

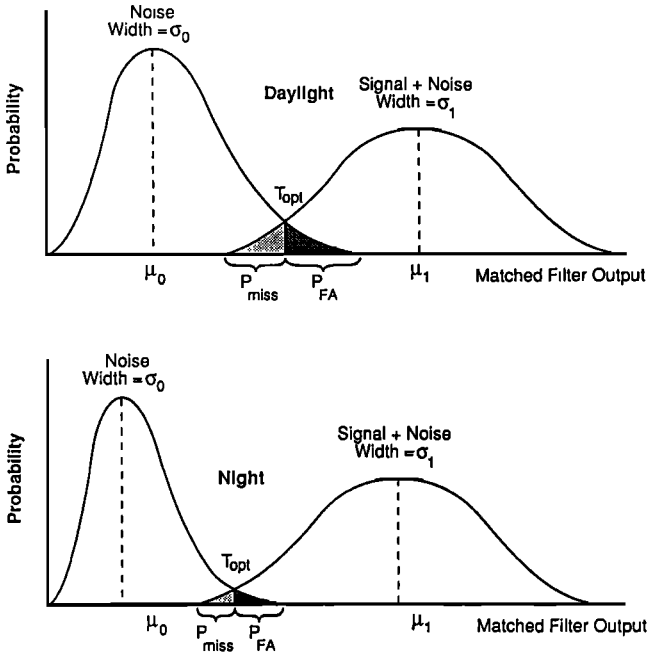

Fig. 7. Schematic illustration of altimetry receiver probability density distributions for day and night conditions. The tracking algorithm of the Mars Observer laser altimeter (MOLA) is designed to minimize the probabilities of missed detections P_{miss} and false alarms P_{FA} (corresponding to the shaded intersections of the probability distributions), thereby maximizing the probability of making useful measurements of range P_{det}.

$$N_r = \left(\frac{E_t \eta}{h\nu}\right)\left(\frac{A_r}{Z^2}\right) t_{sys} t_{atm}^2 \left(\frac{r_{tar}}{\Omega_{tar}}\right) \tag{3}$$

where E_t is the transmitted laser energy, η is the quantum efficiency of the detector, $h\nu$ is the photon energy, A_r is the telescope area, Z is the range from the MO spacecraft to Mars, t_{sys} is the system transmission, t_{atm} is the atmospheric transmission ($t_{atm} = e^{-\tau}$, where τ is opacity), Ω_{tar} is the target scattering angle, and r_{tar} is the target diffuse reflectivity. Typical values of these parameters are given in Table 4. For these values the average number of photoelectrons received when ranging to silicate terrain and dusty ice surfaces are N_r = 756 and 1450, respectively.

On the basis of analyses of 100-m-scale slopes on the lunar highlands and maria derived from stereophotogrammetry [*Moore et al.*, 1980] and of 100-m-scale slopes of pristine volcanic terrains on Earth [*Garvin and Bufton*, 1990], it is anticipated that the slopes to which the altimeter receiver filters are matched span most of the footprint-scale topographic variance on the Martian surface. Figure 8 shows the calculated link margin in decibels as a function of received pulse width for each of the filter channels for returns from terrain and ice surfaces. The calculation assumes a constant false alarm rate. In practice this is maintained by varying the threshold settings of each discriminator once per second by using a computer algorithm that utilizes the background noise counts. Functional tests using the MOLA engineering model and flight unit indicate that under assumed normal atmospheric conditions and the maximum expected solar background during the day, ranging should be possible over both terrain and ice during day and night. For signals with the same pulse width, the signal link margin on the nightside is expected to be approximately 4 dB greater than on the dayside owing to the lower level of the 1064-nm solar background. Consequently, during the day under worse-than-expected ranging and instrument performance conditions, MOLA will range to terrain surfaces with footprint-scale slopes greater than a few degrees with less than 1 dB signal margin at the measurement probabilities given in Table 3, though margins will be greater for lower ranging probabilities. Also note that the measurement probabilities decrease from 0.9 for channels 1 and 2 to 0.5 and 0.1 for channels 3 and 4, respectively. Thus, as illustrated in Figure 3, fewer measurements of range will be obtained on steeply sloping surfaces than on shallowly sloping surfaces. This is a result of the lower received peak power in those signals.

MOLA may be unable to detect some terrain or ice surfaces even at night during dense dust storms or in the presence of thick ground fogs or clouds, such as the polar hoods. However, the instrument has the potential to measure, for the first time, the heights of certain dense ground fogs or other H_2O ice-rich atmospheric layers that contain predominantly backscattering particles. Since atmospheric layers are diffuse reflectors, backscattered laser energy from such features would be considerably spread in time and would be detectable only with MOLA's widest matched filter channel (540 ns; channel 4) and only when operating at night. Consider the idealized case of a thin, low-opacity ($\tau <$ 1) cloud of thickness z_c composed of N single-scattering particles with mean scattering cross section $\bar{\sigma}$. The ratio R of the cloud return signal to a nominal signal returned from the surface can be estimated from

$$R = \frac{cT_w\left(\frac{\tau_c}{z_c}\right)\Omega_{tar}}{8\pi r_{tar} e^{-2\tau_{atm}}} \tag{4}$$

where c is the speed of light, T_w is the matched filter width, τ_c is the cloud opacity, $\Omega_{tar}(= \pi)$ is the scattering solid angle, $\tau_{atm}(= 0.5)$ is the opacity of the Martian atmosphere, and $r_{tar}(= 0.25)$ is the surface electrical reflectivity. For water ice clouds ranging in thickness from 1 to 10 km, $0.07 > R > 0.01$. For values in this range, cloud returns will be difficult to detect, although detection of some nightside returns is possible. Stronger returned signals would be expected for clouds with large opacities (for which (4) is invalid), for multiply scattering particles, and for conservative scattering from nonabsorbing particles. Clearly, more detailed calculations will have to be performed to assess the ability of MOLA to range to atmospheric layers.

TABLE 4. Parameters Assumed in Link Analysis

Symbol	Parameter	Value
E_t, mJ	transmit laser energy	40
η, pe ph^{-1}	APD quantum efficiency	0.3
$h\nu$, J ph^{-1}	photon energy	1.87×10^{-19}
A_r, m^2	receiver telescope area	1.91×10^{-1}
R, km	range to Mars	410
t_{sys}	system transmission	0.5
t_{atm}	atmospheric transmission	0.5
Ω_{tar}, sr	target scattering angle	π
r_{tar}	target diffuse reflectivity	
	silicate terrain	0.26
	ice	0.5

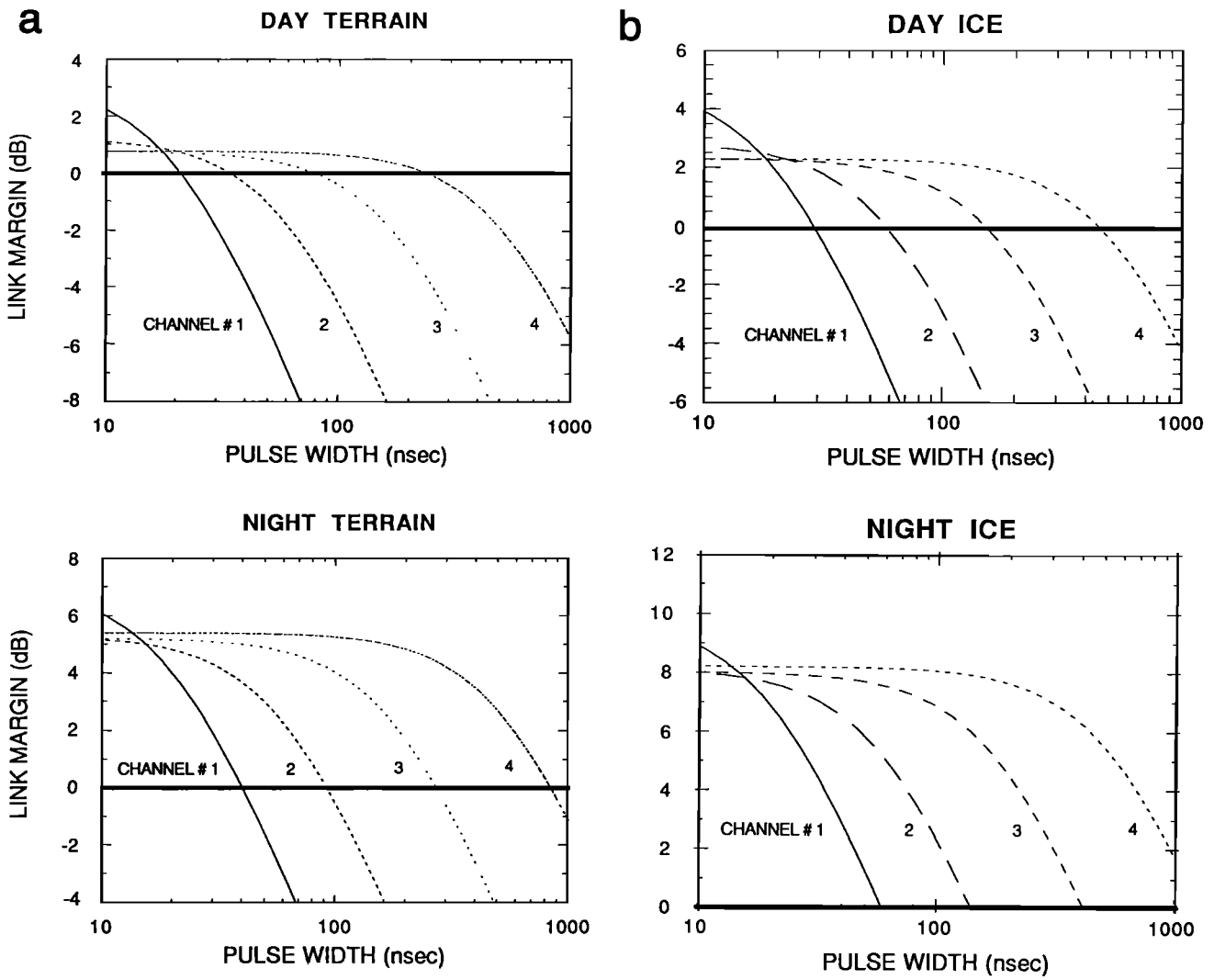

Fig. 8. Link margins plotted in decibels as a function of laser pulse width in nanoseconds for the four matched filter channels in the Mars Observer laser altimeter (MOLA) receiver. Calculations are shown for day and night conditions for signal returns from (*a*) terrain and (*b*) dusty ice (compare Table 4). Results were calculated for the filter characteristics and measurement probabilities in Table 3 and the system and environmental parameters in Table 4. The calculations indicate that under nominal atmospheric conditions, ranging will be possible on both terrain and ice during day and night. Because of the reduced solar background the returned signal strength is approximately 4 dB greater at night than during the day.

Range Gate

To ensure adequate link margin during the Martian day, the width and position of the range gate (Figure 5) was designed to be adjustable around the time of the expected signal return. The range gate width takes into account the expected dynamic range of along-track topography and variations in the orbital altitude of the spacecraft. A wide range gate minimizes the probability of losing a range measurement, such as due to an unanticipated spacecraft maneuver or a topographic extreme. However, a wide range gate also results in a higher level of detected background radiation at the MOLA wavelength, which increases the probability of triggering the detector due to a false alarm. Background contamination considerations, especially during the day, favor a narrow range gate.

When MOLA first attempts to range to Mars or if the altimeter "loses lock" on the surface, the instrument enters "acquisition mode," where the range gate width may be expanded to up to 320 km. During "tracking mode" the range gate will be set to its minimum width of 20 km unless returns are lost, in which case the gate will be widened. The center of the range gate will be adjusted every 20 shots (every 2 s, corresponding to a 6.6-km distance along the MO orbital track) on the basis of the values of the previously measured ranges. However, 8-s periods (80 shots) are examined in the absence of a statistically significant number of "clustered hits," which are representative of terrain signals.

Figure 9 shows a simulation of MOLA's tracking algorithm for the case of an idealized, extreme instantaneous elevation change. The simulation assumes three returns every 2 s corresponding to a 0.15 measurement probability, which is much lower than MOLA's 0.9 measurement requirement for filter channels 1 and 2. The simulation begins in acquisition mode with a range gate width of 80 km. The range gate narrows to 20 km as the instrument shifts to tracking mode after acquiring the surface. The instrument

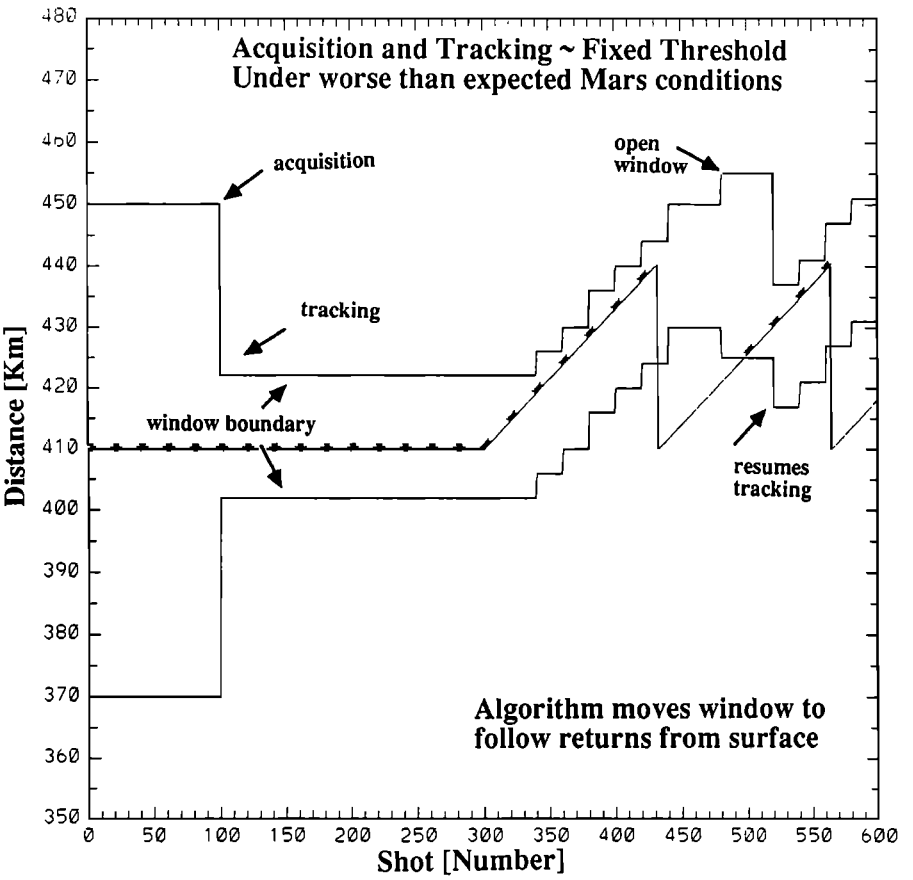

Fig. 9. Simulation of the acquisition and tracking algorithm of the Mars Observer laser altimeter (MOLA) assuming an idealized topographic surface and worse-than-expected Martian conditions. The simulation begins with MOLA in acquisition mode with an 80-km-wide range gate. The range gate narrows to 20 km during tracking mode after the surface has been acquired. The instrument tracks up a 45° slope then misses returns after encountering an instantaneous 30-km elevation change. The range gate widens and the instrument reacquires the signal within several seconds. This simulation assumes detection of three shots per 2 s corresponding to a measurement probability of 0.15, which is significantly less than the measurement requirement of 0.9 for matched filter channels 1 and 2.

tracks up a 45° slope, which is significantly steeper than generally expected on Mars, with the center of the range gate adjusting every 2 s. When the return signal falls outside the range window owing to the encounter of an instantaneous 30-km drop in elevation, the window widens and enables the signal to be reacquired within several seconds. If the signal is not reacquired after opening the window by a specified amount or a specified number of times, the tracking algorithm automatically returns to acquisition mode.

The nominal range gate width of 20 km in tracking mode is large enough that MOLA should continue to track the Martian surface even during the largest near-instantaneous change in topographic elevation, which occurs when crossing the 7-km-deep Valles Marineris. Larger topographic changes such as those associated with the major shield volcanoes, though they may span a range of elevations wider than the range window, are not a problem because these features are characterized by generally low surface slopes (~4°) over baselines of the order of hundreds of kilometers (i.e., much longer than the 6.6-km distance over which the range gate resets). The variations in the orbital altitude occur very slowly and do not stress the range gate algorithm. It is possible that at night, MOLA may also be able to track dense cloud tops or fog tops at altitudes in the lowest scale height of the Martian atmosphere (~10 km) while remaining in tracking mode. Most optically thick atmospheric features observed by the Viking orbiters occur in this altitude range [*Kahn*, 1984; *Lindner*, 1990].

MISSION PLAN

MOLA will undergo a short checkout period during the inner cruise phase of the MO mission at launch + 24 days. The instrument will be powered on, a memory dump and a laser energy test will be performed, noise counts will be measured, and the instrument will then be powered off.

In order to meet the strict mass, power, cost, and time constraints of the investigation, MOLA was designed to have only a single operational science mode. The instrument collects data continuously throughout the MO mapping cycle at the rate of 617.14 bits s^{-1} in 14-s-long packets. Data will be transferred to the MO Payload Data Subsystem (PDS) in packet format for delayed transmission to Earth. Because of the modest data rate there is no need for real-time transmission of data. MOLA may be powered off when no data collection is possible, such as during a global dust storm.

DATA PRODUCTS

If MOLA operates continuously throughout the 687-day MO nominal mission, the instrument will obtain 3.7×10^{10} bits of data. The data will be received by the Deep Space Network and transmitted to the Jet Propulsion Laboratory (JPL) and subsequently to the Goddard Space Flight Center. All processing of MOLA data will be done at Goddard.

The raw MOLA experiment data record (EDR) received from JPL will be processed into several different data products by the science team and transmitted to the MO Project archive. The released MOLA data records will be reduced with different orbits of varying precision depending on the processing stage of the release. The MOLA experiment processed data record (EPDR) will consist of profiles determined using the MO navigation orbits computed by the MO navigation team at the Jet Propulsion Laboratory [*Esposito et al.*, 1990]. These orbits will be determined using a gravity field model complete in spherical harmonics to approximately degree and order 30, and which has been adjusted with 7 days of MO tracking data [*Esposito et al.*, 1990]. The MOLA corrected experiment processed data record (CEPDR) will contain profiles determined using MO precision orbits determined by members of the MO radio science team at the Goddard Space Flight Center [*Tyler et al.*, this issue]. These orbits will be determined using a higher degree and order gravity model (~ degree 50) adjusted with MO tracking data and will therefore likely be much more precise than the MO navigation orbits. All orbits determined for MO will be computed using Doppler tracking data collected by the Deep Space Network (DSN). The final level of processing is the MOLA experiment gridded data record (EGDR), which will consist of global grids of topography, surface slopes, and 1064-nm reflectivity. These grids will also be computed using the MO precision orbits.

Given the characteristics of the Mars Observer orbit, the length of the nominal mapping phase of the mission, and the performance characteristics of MOLA, a global $0.2° \times 0.2°$ grid of topography should ultimately be achievable. Preliminary $5° \times 5°$ and $1° \times 1°$ grids of topography and reflectivity are also planned.

EXPECTED RESULTS

Data provided by MOLA are expected to fulfill the stated Mars Observer altimetry objective [*Mars Observer Science Working Group*, 1987], that is, to define globally the topography of Mars. The MOLA topographic field will consist of a $0.2° \times 0.2°$ grid that will be geodetically referenced with respect to Mars's center of mass with a horizontal positional accuracy of approximately 300 m and a vertical accuracy of approximately 30 m. In addition, MOLA will produce high-resolution local profiles, with an along-track resolution of approximately 300 m and a maximum vertical precision of 1.5 m. The instrument will also provide a global estimate of 1064-nm reflectivity with a precision of approximately ±20%.

In addition, because topographic data are synergistic with visual and multispectral imaging data, with potential field data, and with data pertaining to atmospheric phenomena, MOLA will provide a unique data base from which to make detailed comparisons with other Mars Observer instrument observations. Many key issues in Martian geoscience involve interdisciplinary investigations of the interactive processes between the lithosphere, cryosphere, and atmosphere, and many of these fundamental processes are dependent on absolute elevation, relative relief, or surface slope.

Acknowledgments. We acknowledge the contributions of J. C. Smith, B. L. Johnson, G. H. Pettengill, R. J. Phillips, H. V. Frey, J. G. Marsh, H. J. Zwally, J. B. Blair, J. N. Caldwell, J. S. Chitwood, R. B. Follas, D. W. Hancock, C. W. Kellenbenz, S. S. Manizade, J. F. McGarry, A. Morell, L. K. Pacini, R. Quada, L. Ramos-Izquierdo, W. H. Schaefer, N. E. Schultz, G. L. Unger, R. K. Zimmerman, R. S. Nerem, and W. B. Banerdt to this effort. We thank R. Batson and C. Counselman for helpful reviews, and R. Batson for providing Plate 1. M.T.Z. acknowledges partial support from the Johns Hopkins University Space Research Consortium.

REFERENCES

Albee, A. L., R. E. Arivdon, and F. D. Palluconi, Mars Observer mission, *J. Geophys. Res.*, this issue.

Baker, V. R., *The Channels of Mars*, 198 pp., University of Texas Press, Austin, 1982.

Baker, V. R., and D. J. Milton, Erosion by catastrophic floods on Mars and Earth, *Icarus*, *23*, 27–41, 1974.

Balmino, G., B. Moynot, and N. Valès, Gravity field model of Mars in spherical harmonics up to degree and order eighteen, *J. Geophys. Res.*, *87*, 9735–9746, 1982.

Banerdt, W. B., R. J. Phillips, N. H. Sleep, and R. S. Saunders, Thick shell tectonics on one-plate planets: Applications to Mars, *J. Geophys. Res.*, *87*, 9723–9733, 1982.

Banerdt, W. B., M. P. Golombek, and K. L. Tanaka, Stress and tectonics on Mars, in *Mars*, edited by H. H. Kieffer et al., University of Arizona Press, Tucson, in press, 1992.

Barnes, Possible effects of breaking gravity waves on the circulation of the middle atmosphere of Mars, *J. Geophys. Res.*, *95*, 1401–1421, 1990.

Barth, C. A., and C. W. Hord, Mariner ultraviolet spectrometer: Topography and polar cap, *Science*, *173*, 197–201, 1971.

Bills, B. G., and A. J. Ferrari, Mars topography harmonics and geophysical implications, *J. Geophys. Res.*, *83*, 3497–3508, 1978.

Blasius, K. R., A study of Martian topography by analytical photogrammetry, *J. Geophys. Res.*, *78*, 4411–4423, 1973.

Blasius, K. R., and J. A. Cutts, Topography of Martian central volcanoes, *Icarus*, *45*, 87–112, 1981.

Bufton, J. L., Laser altimetry measurements from aircraft and spacecraft, *Proc. IEEE*, *77*, 463–477, 1989.

Byer, R. L., Diode laser-pumped solid state lasers, *Science*, *239*, 742–747, 1988.

Cain, D. L., A. J. Kliore, B. C. Seidel, and M. J. Sykes, The shape of Mars from the Mariner 9 occultations, *Icarus*, *17*, 517–524, 1972.

Carr, M. H., Volcanism on Mars, *J. Geophys. Res.*, *78*, 4049–4062, 1973.

Carr, M. H., Formation of Martian flood features by release of water from confined aquifers, *J. Geophys. Res.*, *84*, 2995–3007, 1979.

Chapman, C. R., and K. L. Jones, Cratering and obliteration history of Mars, *Annu. Rev. Earth Planet. Sci.*, *5*, 515–540, 1977.

Christensen, E. J., Martian topography derived from occultation, radar, spectral, and optical measurements, *J. Geophys. Res.*, *80*, 2909–2913, 1975.

Christensen, P. R., et al., Thermal Emission Spectrometer Experiment: Mars Observer mission, *J. Geophys. Res.*, this issue.

Comer, R. P., S. C. Solomon, and J. W. Head, Mars: Thickness of the lithosphere from the tectonic response to volcanic loads, *Rev. Geophys.*, *23*, 61–92, 1985.

Cross, P. S., G. L. Harnagel, W. Streifer, D. R. Scifres, and D. F. Welch, Ultrahigh-power semiconductor diode laser arrays, *Science*, *237*, 1305–1309, 1987.

Davies, M. E., and F. Y. Katayama, The 1982 control network of Mars, *J. Geophys. Res.*, *88*, 7503–7504, 1983.

Davies, M. E., R. M. Batson, and S. S. C. Wu, Geodesy and cartography, in *Mars*, edited by H. H. Kieffer et al., University of Arizona Press, Tucson, in press, 1992.

Downs, G. D., R. M. Goldstein, R. R. Green, and G. A. Morris,

Mars radar observations: A preliminary report, *Science*, *174*, 1324–1327, 1971.

Downs, G. D., R. M. Goldstein, R. R. Green, G. A. Morris, and P. E. Reichley, Radar measurements of Martian topography and surface properties, *Icarus*, *18*, 8–21, 1973.

Downs, G. S., P. E. Reichley, and R. R. Green, Radar measurements of Martian topography and surface properties: The 1971 and 1973 oppositions, *Icarus*, *26*, 273–312, 1975.

Downs, G. S., R. R. Green, and P. E. Reichley, Radar studies of the Martian surface at centimeter wavelengths: The 1975 opposition, *Icarus*, *33*, 441–453, 1978.

Downs, G. S., P. J. Mouginis-Mark, S. H. Zisk, and T. W. Thompson, New radar-derived topography for the northern hemisphere of Mars, *J. Geophys. Res.*, *87*, 9747–9754, 1982.

Dyce, R. B., G. H. Pettengill, and A. D. Sanchez, Radar observations of Mars and Jupiter at 70 cm, *Astron. J.*, *72*, 771–777, 1967.

Esposito, P. B., S. Demcak, and D. Roth, Gravity field determination for Mars Observer, *Pap. AIAA, 90-2945*, 621–626, 1990.

Esposito, P. B., W. B. Banerdt, G. F. Lindal, W. L. Sjogren, M. A. Slade, G. Balmino, B. G. Bills, and D. E. Smith, Gravity and topography, in *Mars*, edited by H. H. Kieffer et al., University of Arizona Press, Tucson, in press, 1992.

Fjeldbo, G., D. Sweetnam, D. J. Brenkle, E. Christensen, D. Farless, J. Mehta, B. Seidel, W. Michael, A. Wallio, and M. Grossi, Viking radio occultation measurements of the Martian atmosphere and topography: Primary mission coverage, *J. Geophys. Res.*, *82*, 4317–4324, 1977.

Forsyth, D. W., Subsurface loading and estimates of the flexural rigidity of continental lithosphere, *J. Geophys. Res.*, *90*, 12,623–12,632, 1985.

Frey, H. V., and R. A. Schultz, Large impact basins and the mega-impact origin for the crustal dichotomy on Mars, *Geophys. Res. Lett.*, *15*, 229–232, 1988.

Frey, H. V., and R. A. Schultz, Speculations on the origin and evolution of the Utopia-Elysium lowlands of Mars, *J. Geophys. Res.*, *95*, 14,203–14,213, 1990.

Garvin, J. B., and J. L. Bufton, Lunar Observer Laser Altimeter observations for Lunar Base site selection, in *Proceedings of the 2nd Second Symposium on Lunar Bases in the 21st Century*, edited by W. Mendell, Lunar Planetary Institute, Houston, Tex., in press, 1992.

Garvin, J. B., and R. S. Williams, Small domes on Venus: Probable analogs of Icelandic lava shields, *Geophys. Res. Lett.*, *17*, 1381–1384, 1990.

Goldstein, R. M., Mars radar observations, *Science*, *150*, 1715–1717, 1965.

Goldstein, R. M., and W. F. Gillmore, Radar observations of Mars, *Science*, *41*, 1171–1172, 1963.

Greeley, R., and D. A. Crown, Volcanic geology of Tyrrhena Patera, Mars, *J. Geophys. Res.*, *95*, 7133–7149, 1990.

Greeley, R., and P. D. Spudis, Volcanism on Mars, *Rev. Geophys. Space Phys.*, *19*, 13–41, 1981.

Grimm, R. E., and S. C. Solomon, Viscous relaxation of impact crater relief on Venus: Constraints on crustal thickness and thermal gradient, *J. Geophys. Res.*, *93*, 11,911–11,929, 1988.

Haberle, R. M., and B. M. Jakosky, Sublimation and transport of water from the north residual polar cap of Mars, *J. Geophys. Res.*, *95*, 1423–1437, 1990.

Hall, J. L., S. C. Solomon, and J. W. Head, Elysium region, Mars: Tests of lithospheric loading models for the formation of tectonic features, *J. Geophys. Res.*, *91*, 11,377–11,392, 1986.

Herr, K. C., D. Horn, J. M. McAfee, and G. C. Pimentel, Martian topography from the Mariner 6 and 7 infrared spectra, *Astron. J.*, 883–894, 1970.

Holton, J. R., The influence of gravity wave breaking on the general circulation of the middle atmosphere, *J. Atmos. Sci.*, *40*, 2497–2507, 1983.

Hord, C. W., Mariner 6 and 7 ultraviolet spectrometer experiment: Photometry and topography of Mars, *Icarus*, *17*, 443–456, 1972.

Hord, C. W., K. D. Simmons, and L. K. McLaughlin, Mariner 9 ultraviolet spectrometer experiment: Pressure-altitude measurements on Mars, *Icarus*, *21*, 292–302, 1974.

Hulme, G., The determination of the rheological properties and effusion rate of an Olympus Mons lava, *Icarus*, *27*, 207–213, 1976.

Kahn, R., The spatial and seasonal distribution of Martian clouds and some meteorological implications, *J. Geophys. Res.*, *89*, 6671–6688, 1984.

Kaula, W. M., G. Schubert, R. E. Lingenfelter, W. L. Sjogren, and W. R. Wollenhaupt, Analysis and interpretation of lunar laser altimetry, *Proc. Lunar Sci. Conf.*, *3rd*, 2189–2204, 1972.

Kaula, W. M., G. Schubert, R. E. Lingenfelter, W. L. Sjogren, and W. R. Wollenhaupt, Lunar topography form Apollo 15 and 16 laser altimetry, *Proc. Lunar Sci. Conf.*, *4th*, 2811–2819, 1973.

Kaula, W. M., G. Schubert, R. E. Lingenfelter, W. L. Sjogren, and W. R. Wollenhaupt, Apollo laser altimetry and inferences as to lunar structure, *Proc. Lunar Sci. Conf.*, *5th*, 3049–3058, 1974.

Kliore, A. J., G. Fjeldbo, B. L. Seidel, M. J. Sykes, and P. M. Woiceshyn, S-band radio occultation measurements of the atmosphere and topography of Mars with Mariner 9: Extended mission coverage of the polar and intermediate latitudes, *J. Geophys. Res.*, *78*, 4331–4351, 1973.

Kotelnikov, V. A., V. M. Dubrovich, B. A. Dubinsky, M. D. Kislik, B. I. Kuznetsov, G. M. Petrov, A. P. Rabotiagov, O. N. Rzhiga, and A. M. Shakhovskoi, Radar ranging of Mars in the Soviet Union (in Russian), *Dokl. Akad. Nauk SSSR*, *151*, 811–814, 1963.

Kotelnikov, V. A., et al., 39-cm radar observations of Mars in 1980, *Sov. Astron.*, Engl. Transl., *27*, 246–250, 1983.

Lindal, G. F., H. B. Hotz, D. N. Sweetnam, Z. Shippony, J. P. Brenkle, G. V. Hartsell, R. T. Spear, and W. H. Michael, Jr., Viking radio occultation measurements of the atmosphere and topography of Mars: Data acquired during 1 Martian year of tracking, *J. Geophys. Res.*, *84*, 8443–8456, 1979.

Lindner, B. L., The Martian polar cap: Radiative effects of ozone, clouds, and airborne dust, *J. Geophys. Res.*, *95*, 1367–1379, 1990.

Lopes, R. M. C., and C. R. Kilburn, Emplacement of lava flow shields: Application of terrestrial studies to Alba Patera, Mars, *J. Geophys. Res.*, *95*, 14,383–14,397, 1990.

Mars Observer Science Working Group, Mars Observer spacecraft expected capabilities, *Rep. JPL D-6592*, Jet Propul. Lab., Pasadena, Calif., 1989.

Mars Observer Science Working Group, *Rep. JPL D-2244*, Jet Propul. Lab., Pasadena, Calif., 1987.

McArthur, J. L., SEASAT-A radar altimeter design description, *Tech. Rep. SDO-5232*, Appl. Phys. Lab., Johns Hopkins Univ., Baltimore, Md., 1978.

McGill, G. E., and A. M. Dimitriou, Origin of the Martian global dichotomy by crustal thinning in the late Noachian or early Hesperian, *J. Geophys. Res.*, *95*, 12,595–12,605, 1990.

McGovern, P. J., and S. C. Solomon, State of stress and eruption characteristics of Martian volcanoes (abstract), *Lunar Planet. Sci.*, *21*, 765–766, 1990.

Moore, H. J., D. W. G. Arthur, and G. G. Schaber, Yield strengths of flows on Earth, Mars, and Moon, *Proc. Lunar Planet. Sci. Conf.*, *9th*, 3351–3378, 1978.

Moore, H. J., J. M. Boyce, G. Schaber, and D. Scott, Lunar remote sensing and measurements, *U.S. Geol. Surv. Prof. Pap.*, *1046-B*, B1–B78, 1980.

Mouginis-Mark, P. J., S. H. Zisk, and G. S. Downs, Ancient and modern slopes in the Tharsis region of Mars, *Nature*, *297*, 546–550, 1982.

Mouginis-Mark, P. J., L. Wilson, and M. T. Zuber, The physical volcanology of Mars, in *Mars*, edited by B. J. Jakosky et al., University of Arizona Press, Tucson, in press, 1992.

Pettengill, G. H., C. C. Counselman, L. P. Rainville, and I. I. Shapiro, Radar measurements of Martian topography, *Astron. J.*, *74*, 461–482, 1969.

Pettengill, G. H., A. E. E. Rogers, and I. I. Shapiro, Martian craters and scarp seen by radar, *Science*, *174*, 1321–1324, 1971.

Pettengill, G. H., I. I. Shapiro, and A. E. E. Rogers, Topography and radar scattering properties of Mars, *Icarus*, *18*, 22–28, 1973.

Phillips, R. J., and J. Dvorak, The origin of lunar mascons: Analysis of the Bouguer gravity associated with Grimaldi, in *Multi-ring Basins, Proceedings of the 12th Lunar and Planetary Science Conference*, edited by P. H. Schultz and R. B. Merrill, pp. 91–104, Lunar Planetary Institute, Houston, Tex., 1981.

Phillips, R. J., and K. Lambeck, Gravity fields of the terrestrial planets: Long wavelength anomalies and tectonics, *Rev. Geophys.*, *18*, 27–76, 1980.

Phillips, R. J., and R. S. Saunders, The isostatic state of Martian topography, *J. Geophys. Res.*, *80*, 2893–2898, 1975.

Pike, R. J., Size-dependence in the shape of fresh impact craters on

the Moon, in *Impact and Explosion Cratering*, edited by D. J. Roddy et al., pp. 489–509, Pergamon, New York, 1977.

Pollack, J. B., The general circulation of the Martian atmosphere: A review (abstract), in *Abstracts of the Fourth International Conference on Mars*, pp. 48–49, University of Arizona Press, Tucson, 1989.

Pollack, J. B., D. S. Colburn, F. M. Flaser, R. Kahn, C. E. Carlson, and D. Pidek, Properties and effects of dust particles suspended in the Martian atmosphere, *J. Geophys. Res.*, *84*, 2929–2945, 1979.

Pollack, J. B., C. B. Leovy, P. W. Greiman, and Y. Mintz, A Martian general circulation experiment with large topography, *J. Atmos. Sci.*, *38*, 3–29, 1981.

Roth, L. E., G. S. Downs, R. S. Saunders, and G. Schubert, Radar altimetry of south Tharsis, Mars, *Icarus*, *42*, 287–316, 1980.

Scheiddeger, A. E., *Theoretical Geomorphology*, 435 pp., Springer-Verlag, New York, 1970.

Schubert, G. G., D. Bercovici, and G. A. Glatzmaier, Mantle dynamics in Mars and Venus: Influence of an immobile lithosphere on three-dimensional mantle convection, *J. Geophys. Res.*, 14,105–14,129, 1990.

Schultz, P. H., and A. B. Lutz, Polar wandering on Mars, *Icarus*, *73*, 91–141, 1988.

Sharp, R. P., and M. C. Malin, Channels on Mars, *Geol. Soc. Am. Bull.*, *86*, 593–609, 1975.

Simpson, R. A., G. L. Tyler, and H. T. Howard, Crater morphometry from bistatic radar, in *Impact and Explosion Cratering*, edited by D. J. Roddy, R. O. Pepin, and R. B. Merrill, pp. 481–487, Pergamon, New York, 1977.

Sjogren, W. L., and R. N. Wimberly, Mars: Hellas Planitia gravity analysis, *Icarus*, *45*, 331–338, 1981.

Sleep, N. H., and R. J. Phillips, Gravity and lithospheric stress on the terrestrial planets with reference to the Tharsis region of Mars, *J. Geophys. Res.*, *90*, 4469–4489, 1985.

Smith, D. E., M. T. Zuber, J. B. Garvin, J. L. Bufton, and J. B. Abshire, The Mars Observer Laser Altimeter (MOLA) (abstract), in *Abstracts of the Fourth International Conference on Mars*, pp. 191–192, University of Arizona Press, Tucson, 1989.

Smith, D. E., F. J. Lerch, J. C. Chan, D. S. Chinn, H. B. Iz, A. Mallama, and G. B. Patel, Mars gravity field error analysis from radio tracking of Mars Observer, *J. Geophys. Res.*, *95*, 14,115–14,167, 1990*a*.

Smith, D. E., F. J. Lerch, R. S. Nerem, G. B. Patel, and S. K. Fricke, Developing an improved higher resolution gravity field model for Mars (abstract), *Eos Trans. AGU*, *71*, 1427, 1990*b*.

Solomon, S. C., and J. W. Head, Evolution of the Tharsis province, Mars: The importance of heterogeneous lithospheric thickness and volcanic construction, *J. Geophys. Res.*, *87*, 9755–9774, 1982.

Solomon, S. C., and J. W. Head, Heterogeneities in the thickness of the elastic lithosphere of Mars: Constraints on heat flow and internal dynamics, *J. Geophys. Res.*, *95*, 11,073–11,083, 1990.

Solomon, S. C., R. P. Comer, and J. W. Head, The evolution of impact basins: Viscous relaxation of topographic relief, *J. Geophys. Res.*, *87*, 3975–3992, 1982.

Solomon, S. C., W. L. Sjogren, and S. R. Bratt, The structure of the Isidis Basin, Mars, from gravity anomalies (abstract), *Lunar Planet. Sci.*, *14*, 725–726, 1983.

Tanaka, K. L., N. K. Isbell, D. H. Scott, R. Greeley, and J. E. Guest, The resurfacing history of Mars: A synthesis of digitized, Viking-based geology, *Proc. Lunar Planet. Sci. Conf.*, *18th*, 665–678, 1988.

Tyler, G. L., G. Balmino, D. P. Hinson, W. L. Sjogren, D. E. Smith, R. Woo, S. W. Asmar, M. J. Connally, C. L. Hamilton, and R. A. Simpson, Radio science investigations with Mars Observer, *J. Geophys. Res.*, this issue.

U.S. Geological Survey, Topographic maps of the western, eastern equatorial and polar regions of Mars, scale 1:15,000,000, *Map I-2030*, 1989.

Walcott, R. I., Flexural rigidity, thickness and viscosity of the lithosphere, *J. Geophys. Res.*, *75*, 349–369, 1970.

Wilhelms, D. E., and S. W. Squyres, The Martian hemispheric dichotomy may be due to a giant impact, *Nature*, *309*, 138–140, 1984.

Willemann, R. J., and D. L. Turcotte, The role of lithospheric stress in the support of the Tharsis bulge, *J. Geophys. Res.*, *87*, 9793–9801, 1982.

Wilson, L., and J. W. Head, III, Ascent and eruption of basaltic magma on the Earth and Moon, *J. Geophys. Res.*, *86*, 2971–3001, 1981.

Wise, D. U., M. P. Golombek, and G. E. McGill, Tharsis province of Mars: Geologic sequence, geometry, and a deformation mechanism, *Icarus*, *38*, 456–472, 1979.

Wu, S. S. C., Mars synthetic topographic mapping, *Icarus*, *33*, 417–440, 1978.

Wu, S. C. C., Photogrammetric portrayal of Mars topography, *J. Geophys. Res.*, *84*, 7955–7959, 1979.

Wu, S. S. C., F. J. Schafer, G. M. Nakata, R. Jordan, and K. R. Blasius, Photogrammetric evaluation of Mariner 9 photography, *J. Geophys. Res.*, *78*, 4405–4410, 1973.

Wu, S. S. C., P. A. Garcia, R. Jordan, F. J. Schafer, and B. A. Skiff, Topography of the shield volcano, Olympus Mons on Mars, *Nature*, *309*, 432–435, 1984.

Wu, S. S. C., R. Jordan, and F. J. Schafer, Mars global topographic map 1:15,000,000 scale, *NASA Tech. Memo.*, *TM-88383*, 614–617, 1986.

Zuber, M. T., Should lithospheric flexure due to the load of the Martian polar layered deposits be detectable with the Mars Observer laser altimeter? (abstract), *Lunar Planet. Sci.*, *22*, 1593–1594, 1992.

Zwally, H. J., A. C. Brenner, J. A. Major, R. A. Bindschadler, and J. G. Marsh, Growth of the Greenland ice sheet: Measurement, *Science*, *246*, 1587–1589, 1989.

J. B. Abshire, J. L. Bufton, J. B. Garvin, D. E. Smith, and M. T. Zuber, Laboratory for Terrestrial Physics, NASA Goddard Space Flight Center, Greenbelt, MD 20771.

J. W. Head, Department of Geological Sciences, Box 1846, Brown University, Providence, RI 02912.

D. O. Muhleman, Division of Geological and Planetary Sciences, California Institute of Technology, Pasadena, CA 91125.

S. C. Solomon, Department of Earth, Atmospheric, and Planetary Sciences, 54-522, Massachusetts Institute of Technology, Cambridge, MA 02139.

(Received May 6, 1991;
revised February 10, 1992;
accepted February 12, 1992.)